American Mineralogist, Volume 79, pages 826–837, 1994

Temperature-dependent electron delocalization in $(Mg,Fe)SiO_3$ perovskite

Y. Fei, D. Virgo, B. O. Mysen
Center for High Pressure Research and Geophysical Laboratory, 5251 Broad Branch Road, NW, Washington, DC 20015, U.S.A.
Y. Wang
Center for High Pressure Research and Department of Earth and Space Sciences, SUNY, Stony Brook, New York 11794, U.S.A.
H. K. Mao
Center for High Pressure Research and Geophysical Laboratory, 5251 Broad Branch Road, NW, Washington, DC 20015, U.S.A.

Abstract

The oxidation state and location of Fe in the structure of two Fe-bearing silicate perovskite samples, with compositions $Mg_{0.95}Fe_{0.05}SiO_3$ and $Mg_{0.90}Fe_{0.10}SiO_3$, have been studied with ^{57}Fe Mössbauer spectroscopic techniques over the temperature range 30–450 K.

At low temperatures, the resonant absorption spectra consist of a broad absorption envelope due to discrete Fe^{2+} valencies. The line shape of this envelope is the sum of contributions from different local electronic environments. Superimposed on the Fe^{2+} absorption envelope is a partially resolved, narrow, quadrupole split doublet due to discrete Fe^{3+} valencies. The molar Fe^{3+}/Fe_{tot} is about 0.12 ($\pm$0.02) for both samples. At temperatures above 180 and 77 K for the $Mg_{0.95}Fe_{0.05}SiO_3$ and $Mg_{0.90}Fe_{0.10}SiO_3$ compositions, respectively, there is a systematic increase in the relative intensity of an additional broad absorption pattern with intermediate hyperfine parameters between those of Fe^{2+} and Fe^{3+}. This broad absorption is attributed to thermally activated Fe^{2+}-Fe^{3+} electron delocalization.

The hyperfine parameters of Fe^{3+} are consistent with octahedral coordination. Fe^{2+} in the structure is assigned to the distorted eight- to 12-fold-coordinated polyhedra on the basis of the hyperfine parameters and bond distances in agreement with the interpretation of the electron delocalization. The electron exchange most likely occurs between face-sharing Fe^{3+}-bearing octahedra and distorted Fe^{2+}-bearing polyhedra in the perovskite structure. These crystallographically distinct sites have the shortest M-M distances.

The activation energy of Fe^{2+}-Fe^{3+} exchange processes in silicates and oxides is compatible with the result expected from a mechanism associated with electrical conduction in perovskite. An electron-hopping mechanism may thus be important in explaining the conductivity profile determined from geomagnetic data.

Introduction

High-pressure and high-temperature phase equilibrium studies in the system MgO-FeO-SiO_2 have shown that $(Mg,Fe)SiO_3$ perovskite is the only stable Fe-bearing silicate phase in the lower mantle (e.g., Liu and Bassett, 1986; Jeanloz and Thompson, 1983). Characterization of the crystal chemistry of Fe in the $(Mg,Fe)SiO_3$ perovskite structure is essential, therefore, to an understanding of lower mantle properties such as electrical conductivity and heat transfer.

The structure and crystal chemistry of $MgSiO_3$ perovskite have been extensively studied by powder X-ray diffraction (Yagi et al., 1978; Ito and Matsui, 1978), by single-crystal X-ray diffraction techniques (Horiuchi et al., 1987), and by ^{29}Si MAS NMR spectroscopic techniques (Kirkpatrick et al., 1991). Results from these studies have shown that $MgSiO_3$ perovskite has an orthorhombic structure (space group *Pbnm*), with Si in very symmetrical octahedral and Mg in distorted eight- to 12-fold-coordinated polyhedra. The effect of Fe on the crystal structure of $MgSiO_3$ perovskite has been studied with various techniques, including extended X-ray absorption fine structure (EXAFS) (Jackson et al., 1987), X-ray absorption near-edge spectroscopy (XANES) (Parise et al., 1990), single-crystal X-ray diffraction techniques (Kudoh et al., 1990), high-resolution powder X-ray diffraction (Parise et al., 1990), ^{57}Fe Mössbauer spectroscopy (Jeanloz et al., 1992; McCammon et al., 1992; Fei et al., 1992), and optical absorption spectroscopy (Shen et al., 1994).

From EXAFS and ^{57}Fe Mössbauer spectroscopic measurements on $Mg_{0.90}Fe_{0.10}SiO_3$ perovskite synthesized in a diamond-anvil cell by laser heating, Jackson et al. (1987) and Jeanloz et al. (1992) proposed that Fe^{2+} substitutes for Si in the octahedral site, thereby requiring some Si to be in the larger and more distorted polyhedral sites. This suggestion is, however, contrary to the single-crystal and high-resolution powder X-ray diffraction results of Ku-

0003–004X/94/0910–0826$02.00

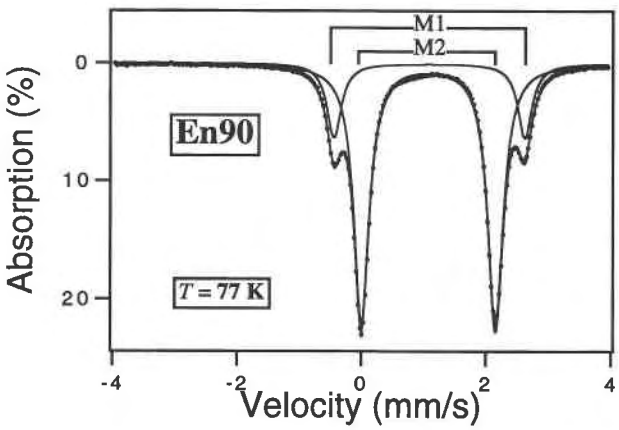

Fig. 1. The ^{57}Fe Mössbauer spectra of orthopyroxene with composition $Mg_{0.90}Fe_{0.10}SiO_3$ at 77 K. Outer and inner doublets are due to Fe^{2+} in M1 and M2 sites, respectively. The solid line is the least-squares fitted line assuming Lorentzian line shape to the folded and uncorrected count rates.

TABLE 1. Bond length at ambient conditions and hyperfine parameters at 77 K for Fe^{2+} in perovskite, orthopyroxene, and garnet structures

Site	Cation	Bond length (Å)	Quadrupole splitting (mm/s)	Isomer shift (mm/s)
		(Mg,Fe)SiO_3 perovskite		
6	Si	1.78–1.81*		
8–12	Mg,Fe^{2+}	2.01–3.12*	1.5–2.6**	1.26–1.29**
		orthopyroxene, $FeSiO_3$		
M1(6)	Fe^{2+}	2.08–2.19†	3.11†	1.29†
M2(6)	Fe^{2+}	2.00–2.58†	2.04†	1.26†
		orthopyroxene, $Mg_{0.9}Fe_{0.1}SiO_3$		
M1(6)	Mg,Fe^{2+}	2.01–2.17‡	3.06**	1.28**
M2(6)	Mg,Fe^{2+}	1.99–2.45‡	2.15**	1.27**
		garnet		
8	Mg,Fe^{2+}	2.20–2.34‡	3.62–3.70§	1.41–1.44§

* Kudoh et al. (1990).
** This study.
† Burnham et al. (1971).
‡ Smyth and Bish (1988).
§ Luth et al. (1990).

doh et al. (1990) and Parise et al. (1990) on (Mg,Fe)SiO_3 perovskite synthesized in a multianvil apparatus. McCammon et al. (1992) also showed that the hyperfine parameters determined from ^{57}Fe Mössbauer spectra of $Mg_{0.95}Fe_{0.05}SiO_3$ perovskite synthesized in the presence of Fe metal in a multianvil device were consistent with Fe^{2+} in the eight- to 12-fold-coordinated site in the perovskite structure.

The perovskites used in the studies of Jeanloz et al. (1992) and McCammon et al. (1992) each have different Fe/(Mg + Fe) and Fe^{3+} contents. To evaluate systematically the effect of Fe on the crystal chemistry of perovskite, two samples with different Fe/(Mg + Fe) and similar Fe^{3+} contents have been synthesized in a multianvil apparatus. The oxidation and structural state of Fe were determined using ^{57}Fe Mössbauer spectroscopic techniques over the temperature range of 30–450 K.

Sample synthesis and characterization

Two (Mg,Fe)SiO_3 perovskite samples, with Fe/(Fe + Mg) ratios of 0.05 and 0.10, were synthesized in the multianvil apparatus at the Center for High Pressure Research and Mineral Physics Institute, SUNY at Stony Brook. The starting materials were ^{57}Fe-enriched (92% enrichment) $Mg_{0.95}Fe_{0.05}SiO_3$ and $Mg_{0.90}Fe_{0.10}SiO_3$ orthopyroxenes synthesized in a piston cylinder apparatus at 1.5 GPa and 1273 K. The ^{57}Fe Mössbauer spectrum of the $Mg_{0.90}Fe_{0.10}SiO_3$ orthopyroxene at 77 K is shown in Figure 1. Its quadrupole splitting and isomer shift (Table 1) are consistent with the expected values for Fe^{2+} in the M1 and M2 sites of the orthopyroxene structure (e.g., Virgo and Hafner, 1969). The Fe^{2+} absorption doublets are well resolved. The relative intensities of the doublets are indicative of a high degree of Fe^{2+} disorder between M1 and M2 sites (cf. Virgo and Hafner, 1969).

The powdered starting materials were packed into a Re capsule 1.2 mm in diameter and 3 mm in length, which also served as a heater. A lanthanum chromite sleeve outside this heater provided thermal insulation. A detailed description of the cell assembly was given by Wang et al. (1992). The two perovskite samples were synthesized at 26 GPa and at 1873 and 1923 K for the $Mg_{0.95}Fe_{0.05}SiO_3$ and $Mg_{0.90}Fe_{0.10}SiO_3$ compositions, respectively.

Both samples were examined optically and with high-resolution powder X-ray diffraction techniques. The unit-cell volumes for the $Mg_{0.95}Fe_{0.05}SiO_3$ and $Mg_{0.90}Fe_{0.10}SiO_3$ perovskites are 162.80(1) and 163.09(1) $Å^3$, respectively. These values are consistent with the unit-cell parameters determined as a function of the Fe content for (Mg,Fe)SiO_3 (Kudoh et al., 1990). Their bulk compositions, determined with the electron microprobe, were $Mg_{0.951(7)}Fe_{0.050(5)}Si_{0.999(4)}O_3$ and $Mg_{0.906(10)}Fe_{0.097(5)}Si_{0.997(5)}O_3$.

Experimental procedure

The ^{57}Fe Mössbauer spectra were collected with an Austin Science drive operated in the constant acceleration mode with a symmetrical wave form. The velocity ramp to the drive was approximately ±4 mm/s. Mirror-imaged spectra were recorded over 512 channels. Velocity vs. channel number was calibrated by the positions of the inner four peaks of Fe metal using values of g_0 = 3.9156 and g_1 = 2.2363 (Stevens and Stevens, 1972). The full widths at half height (FWHH) were about 0.28 and 0.26 mm/s for the inner and outer lines of the Fe foil, respectively. The source was about 38 mCi ^{57}Co in Pd.

To obtain low-temperature Mössbauer spectra, a closed-cycle refrigerator (model CSW202A from ARS cryogenics, Allentown, Pennsylvania) was used. The refrigerator provides sample cooling by the expansion of He gas. The control temperature vs. the sample temperature was calibrated over the experimental temperature range 10–330 K. The maximum deviation of the sample temperature from the control temperature was 20 K at a control temperature of 10 K. This difference decreased to zero at 200 K. Possible line broadening was assessed by comparing low-temperature data obtained on Fe-rich orthopyroxene

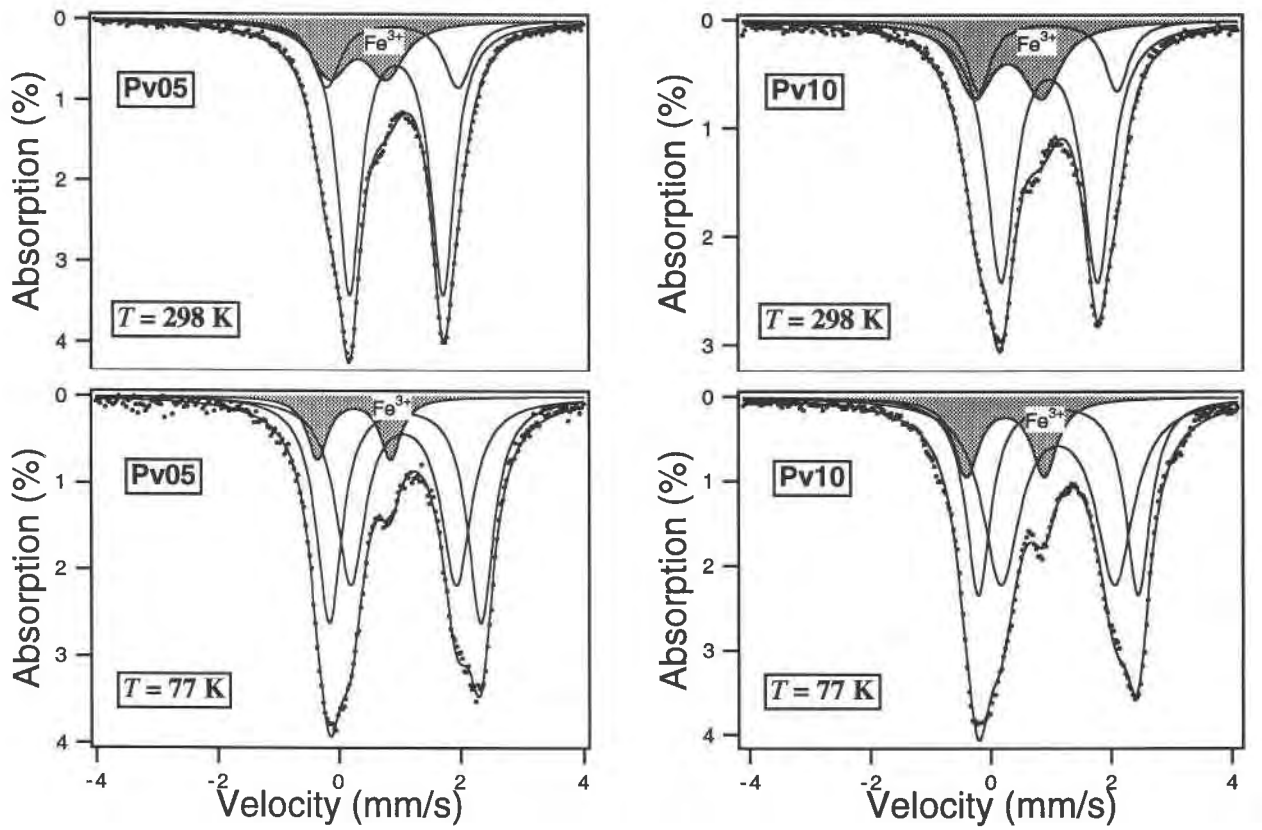

Fig. 2. The ^{57}Fe Mössbauer spectra of $Mg_{0.95}Fe_{0.05}SiO_3$ (labeled as Pv05) and $Mg_{0.9}Fe_{0.1}SiO_3$ (labeled as Pv10) perovskites at 298 and 77 K. The spectra were fitted with two Fe^{2+} doublets and one Fe^{3+} doublet (three-doublet model) using Lorentzian line shape. The shaded area indicates the absorption doublet due to Fe^{3+}.

using the closed-cycle refrigerator with data collected in a traditional liquid-N_2 cryostat (Virgo and Hafner, 1969). In both experiments, the spectral data were measured on a ½-in. pellet of sample mixed with transoptic powder (Virgo and Hafner, 1969). At 77 K, the fitted widths for the low- and high-velocity peaks of the doublets assigned to M1 and M2 sites are, respectively, 0.287, 0.275, and 0.320, 0.329 mm/s, which are comparable to the results obtained by using a traditional cryostat (cf. Burnham et al., 1971). The resolution of the doublets due to Fe^{2+} in M1 and M2 sites is identical to that obtained by Burnham et al. (1971) with the same orthopyroxene sample. The area ratio M1/(M1 + M2) obtained in this study is 0.429, compared with 0.426 obtained in the previous study (e.g., Burnham et al., 1971). A cryostat identical to that used by Virgo and Hafner (1969) was also used to obtain spectral data on perovskites at 77 K.

High-temperature spectra at 400 and 450 K were obtained by heating the sample in a cylinder-shaped $Ni_{80}Cr_{20}$-wire resistance heater. In these high-temperature experiments, the sample temperature was measured with a chromel-alumel thermocouple glued to the surface of the sample container.

To prepare the pellet for Mössbauer spectroscopy, the synthesized perovskite samples were crushed between two WC anvils in a small piston cylinder device. The device was precooled to 77 K to prevent amorphization of the samples during crushing. The powdered samples were then sandwiched between two high-purity Al foils, which were glued to a Cu disk (~1 mm thick) with a ¼-in. aperture in the center. Approximately 2 mg of $Mg_{0.95}{}^{57}Fe_{0.05}SiO_3$ and 1.5 mg of $Mg_{0.90}{}^{57}Fe_{0.10}SiO_3$ perovskite powder samples were used in the Mössbauer experiments. The absorber densities were in the range 7–10 mg natural Fe per square centimeter. This sample assembly was contained in a Cu block in the liquid-N_2 cryostat (Virgo and Hafner, 1969). In the closed-cycle refrigerator, the sample assembly was compressed between the faces of two Cu disks with a ¾-in. aperture, each lined with In foil and then attached to the cold finger of the cryostat.

Spectral data on the perovskite samples were first collected at room temperature (298 K) and at liquid-N_2 temperature (77 K) with a traditional liquid-N_2 cryostat. In experiments with the closed-cycle refrigerator, spectral data were collected initially at the lowest temperature (control temperature of 10 K) and subsequently at successively higher temperatures to the maximum temperature attainable with this system (330 K). At the end of the experiments, data were collected at 298 K again on the sample removed from the cryostat. The fitted results from the spectra collected at 298 and 77 K are identical to those taken as a function of temperature in the closed-cycle refrigerator, which confirms our temperature calibration in the range 77–298 K. The samples were then

TABLE 2. Quadrupole splitting (QS), isomer shift (IS), and half-width (FWHH) for (Mg,Fe)SiO_3 perovskites: three-doublet fits

No.	T (K)	$Fe^{2+}1$ QS (mm/s)	$Fe^{2+}1$ IS (mm/s)	$Fe^{2+}1$ FWHH (mm/s)	$Fe^{2+}2$ QS (mm/s)	$Fe^{2+}2$ IS (mm/s)	$Fe^{2+}2$ FWHH (mm/s)	Fe^{3+} QS (mm/s)	Fe^{3+} IS (mm/s)	Fe^{3+} FWHH (mm/s)	χ^2
					$Mg_{0.90}Fe_{0.10}SiO_3$ (Pv10)						
151P3	450	2.077	1.020	0.387	1.438	1.019	0.508	1.293	0.464	0.871	1.395
149P3	400	2.186	1.049	0.388	1.494	1.048	0.553	1.292	0.468	0.894	1.423
132P3	330	2.222	1.099	0.448	1.543	1.105	0.544	1.131	0.457	0.808	1.282
266P1*	298	2.264	1.121	0.454	1.580	1.130	0.586	1.103	0.437	0.662	2.552
131P3	280	2.319	1.125	0.487	1.601	1.143	0.561	1.110	0.466	0.763	1.478
130P3	230	2.324	1.182	0.499	1.619	1.175	0.558	1.157	0.441	0.634	1.679
129P3	181	2.410	1.224	0.485	1.700	1.204	0.617	1.199	0.421	0.543	1.813
128P3	136	2.485	1.254	0.481	1.771	1.232	0.642	1.238	0.412	0.499	2.243
127P3	113	2.520	1.268	0.509	1.803	1.253	0.679	1.263	0.421	0.475	2.016
126P3	86	2.612	1.278	0.472	1.874	1.266	0.742	1.286	0.409	0.488	3.014
260P1*	77	2.605	1.276	0.486	1.853	1.272	0.733	1.270	0.405	0.498	5.496
					$Mg_{0.95}Fe_{0.05}SiO_3$ (Pv05)						
155P3	450	2.111	1.012	0.406	1.450	1.024	0.455	1.306	0.542	0.839	1.649
153P3	400	2.055	1.008	0.557	1.450	1.059	0.421	1.183	0.609	0.868	1.320
145P3	330	2.150	1.042	0.505	1.503	1.107	0.447	0.854	0.527	0.720	1.207
255P1*	298	2.200	1.052	0.557	1.534	1.126	0.482	0.893	0.502	0.598	1.614
144P3	280	2.205	1.079	0.517	1.554	1.142	0.465	0.818	0.538	0.723	1.294
143P3	230	2.221	1.083	0.497	1.560	1.142	0.472	0.849	0.521	0.724	1.296
142P3	181	2.385	1.152	0.509	1.640	1.201	0.485	0.839	0.568	0.436	1.623
141P3	136	2.295	1.241	0.531	1.684	1.227	0.504	1.144	0.432	0.407	1.343
140P3	113	2.373	1.254	0.510	1.732	1.239	0.541	1.186	0.434	0.398	1.688
139P3	86	2.449	1.265	0.510	1.766	1.251	0.552	1.195	0.422	0.428	1.267
245P1*	77	2.499	1.265	0.508	1.738	1.242	0.591	1.214	0.421	0.410	1.649
138P3	73	2.507	1.269	0.484	1.822	1.262	0.604	1.194	0.416	0.380	1.861
137P3	56	2.557	1.268	0.500	1.839	1.264	0.633	1.236	0.422	0.499	1.446
136P3	31	2.568	1.266	0.479	1.867	1.266	0.633	1.190	0.423	0.469	1.586

* Spectral data collected in a separate experiment.

placed in the $Ni_{80}Cr_{20}$-wire resistance heater for measurements at temperatures above 330 K.

The folded spectral data were fitted with lines of Lorentzian shape using the computing program PC-MOS (CMTE Elektronik, Auenstraße 15, D-8012 Riemerling, Germany). The background values of the unfolded spectra were ~ 2–3×10^6 counts per channel.

RESULTS

The ^{57}Fe Mössbauer spectra of Fe-bearing silicate perovskite show three resolvable absorption peaks (Fig. 2). The two intense peaks have asymmetric peak shape and become significantly broad at low temperature. Therefore, more than one doublet is required to represent the intense peaks. The third peak is partially resolved at 298 K and becomes better resolved at 77 K (Fig. 2).

As a first attempt in fitting the spectra, the spectral data of both perovskite samples were fitted with two absorption doublets due to Fe^{2+} and one doublet assigned to Fe^{3+}. Fits to the spectral data of the $Mg_{0.95}Fe_{0.05}SiO_3$ and $Mg_{0.90}Fe_{0.10}SiO_3$ perovskites using this three-doublet model are shown in Figure 2. The calculated hyperfine parameters at all temperatures are given in Table 2. In comparison with the absorption spectra of other rock-forming silicates, the two doublets with the largest quadrupole splittings are assigned to Fe^{2+}, whereas the doublet of which only the high-velocity line is usually observed is attributable to Fe^{3+}, on the basis of their isomer shift values. The low-velocity component of the Fe^{3+} doublet can be expected to occur beneath the low-velocity absorption due to Fe^{2+}. This in part explains why the intensity of the cumulative envelope at low velocity below 0 mm/s is greater than that at high velocity.

In these fits, the least-squares fitted line does not pass through all the data points, especially for the room-temperature spectra. There are systematic deviations in the region near 1.2 mm/s (Fig. 2). There are a number of changes in the hyperfine parameters with temperature that suggest that this simplified model is inadequate. For example, the half-width (FWHH) of the Fe^{3+} absorption increases with increasing temperature (Table 2), which is inconsistent with the hyperfine parameters of well-defined crystallographic sites. The isomer shifts of the Fe^{3+} doublet increase with increasing temperature rather than decrease as required by the second-order Doppler-shift variation with temperature. Also, the molar ratio Fe^{3+}/Fe_{tot} calculated from these fits increases with increasing temperature by a factor of almost 2 over the temperature range investigated (Fig. 3 and Table 3). Concomitantly, there is a decrease in the percent of absorption due to Fe^{2+} (Fig. 3 and Table 3). In these three-doublet fits, the more intense absorption due to Fe^{2+} is fitted with two quadrupole split doublets, which could be assigned to two distinct Fe^{2+} environments in the crystal structure. This assumption may be reasonable because the Fe^{2+} absorption broadens at low temperature, which might indicate increasing resolution of the two doublets. However, as shown in Figure 4, the relative intensities of the two Fe^{2+} doublets change with temperature, i.e., the area of the Fe^{2+} doublet with the larger quadrupole splitting ($Fe^{2+}1$ in Tables 2 and 3) increases with decreasing temperature, and the area of Fe^{2+} doublet with the smaller splitting

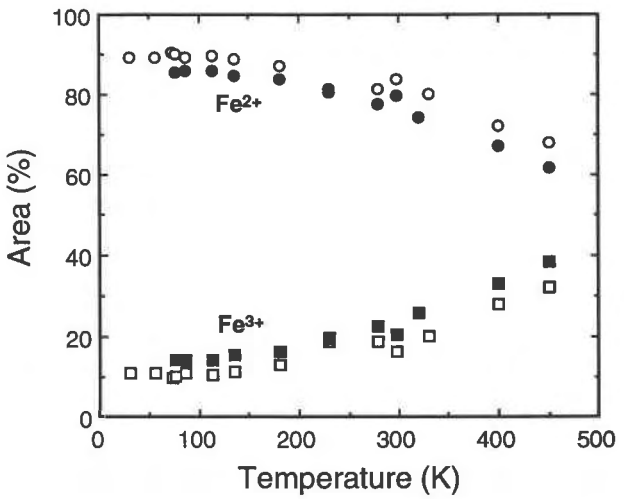

Fig. 3. The Fe^{3+}/Fe_{tot} and Fe^{2+}/Fe_{tot} area percentages vs. temperature for $Mg_{0.95}Fe_{0.05}SiO_3$ (open symbols) and $Mg_{0.9}Fe_{0.1}SiO_3$ (solid symbols) perovskites. The relative intensities were determined from fits to the spectral data using the three-doublet model (Tables 2 and 3).

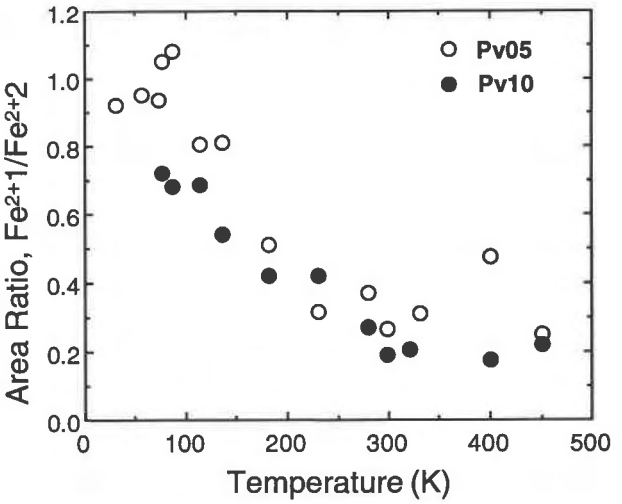

Fig. 4. The area ratios $Fe^{2+}1/Fe^{2+}2$ vs. temperature for $Mg_{0.95}Fe_{0.05}SiO_3$ (labeled as Pv05, open symbols) and $Mg_{0.9}Fe_{0.1}SiO_3$ (labeled as Pv10, solid symbols), calculated from fits to the spectral data using the three-doublet model (Tables 2 and 3).

($Fe^{2+}2$ in Tables 2 and 3) decreases with decreasing temperature. The intensity inversion of the two Fe^{2+} doublets might imply a change in the positional order-disorder of Fe^{2+} in the structure as a function of temperature. However, this possibility is considered unlikely in the temperature range below 298 K.

TABLE 3. Area ratios for $(Mg,Fe)SiO_3$ perovskites: three-doublet fits

No.	*T* (K)	$Fe^{2+}1$ (%)	$Fe^{2+}2$ (%)	$Fe^{2+}1/Fe^{2+}2$	Fe^{2+} (%)	Fe^{3+} (%)
			$Mg_{0.90}Fe_{0.10}SiO_3$ (Pv10)			
151P3	450	11.14	50.49	0.221	61.63	38.37
149P3	400	9.95	57.20	0.174	67.15	32.85
132P3	330	12.63	61.63	0.205	74.26	25.74
266P1*	298	12.64	66.88	0.189	79.52	20.48
131P3	280	16.44	61.24	0.268	77.68	22.32
130P3	230	23.86	56.63	0.421	80.49	19.51
129P3	181	24.69	59.03	0.418	83.72	16.28
128P3	136	29.64	55.01	0.539	84.65	15.35
127P3	113	34.88	50.75	0.687	85.63	14.36
126P3	86	34.81	51.20	0.680	86.01	13.99
260P1*	77	35.90	49.72	0.722	85.62	14.37
			$Mg_{0.95}Fe_{0.05}SiO_3$ (Pv05)			
155P3	450	13.62	54.46	0.250	68.08	31.92
153P3	400	23.17	48.83	0.475	72.00	28.00
145P3	330	19.02	61.05	0.312	80.07	19.92
255P1*	298	17.53	66.07	0.265	83.60	16.40
144P3	280	21.87	59.41	0.368	81.28	18.72
143P3	230	19.48	61.89	0.315	81.37	18.66
142P3	181	29.42	57.81	0.509	87.23	12.77
141P3	136	39.62	48.98	0.809	88.60	11.40
140P3	113	39.94	49.51	0.807	89.45	10.54
139P3	86	46.37	42.85	1.082	89.22	10.78
254P1*	77	46.00	43.85	1.049	89.85	10.15
138P3	73	43.75	46.69	0.937	90.44	9.56
137P3	56	43.46	45.63	0.952	89.09	10.91
136P3	31	42.76	46.44	0.921	89.20	10.79

* Spectral data collected in separate experiment.

In view of the above anomalies, additional models of the spectral data are appropriate. As a next step in the fitting procedure, the spectra were fitted to four quadrupole split doublets, with the high-velocity component of the additional doublet fitted to account for the misfit near 1.2 mm/s. Examples of fitted spectra of both perovskite samples are shown in Figure 5, and the fitted hyperfine parameters are given in Tables 4 and 5. By adding this fourth doublet in the fitting procedure (shaded doublet in Fig. 5), there is a quantitative improvement in the statistical parameters (Tables 4 and 5) relative to the results for the three-doublet model fit (Tables 2 and 3). The Mössbauer parameters of this additional doublet are intermediate between Fe^{2+} and Fe^{3+} (labeled Fe^{n+} in Table 4). Furthermore, the half-width (FWHH) and percent of absorption appear to increase systematically with increasing temperature (Tables 4 and 5).

The anomalous changes in the relative intensities of the two Fe^{2+} doublets as a function of temperature and the increase in line width (FWHH) of each doublet with decreasing temperature are still evident in these four-doublet fits of the spectral data (Tables 4 and 5). The absorption envelope ascribed to Fe^{2+} can be fitted with many additional doublets. Clearly, none of these fits represent a unique solution.

It is proposed that the observed line broadening and changes in the relative intensities of the Fe^{2+} absorption with decreasing temperature are consistent with the presence of different electronic environments due to different next-neighbor populations. In this model, the cumulative envelope of data is the sum of many elemental distributions. These distributions are reflected in a distribution of the hyperfine parameters, principally, the quadrupole splitting. We have fitted the broad Fe^{2+} absorption with

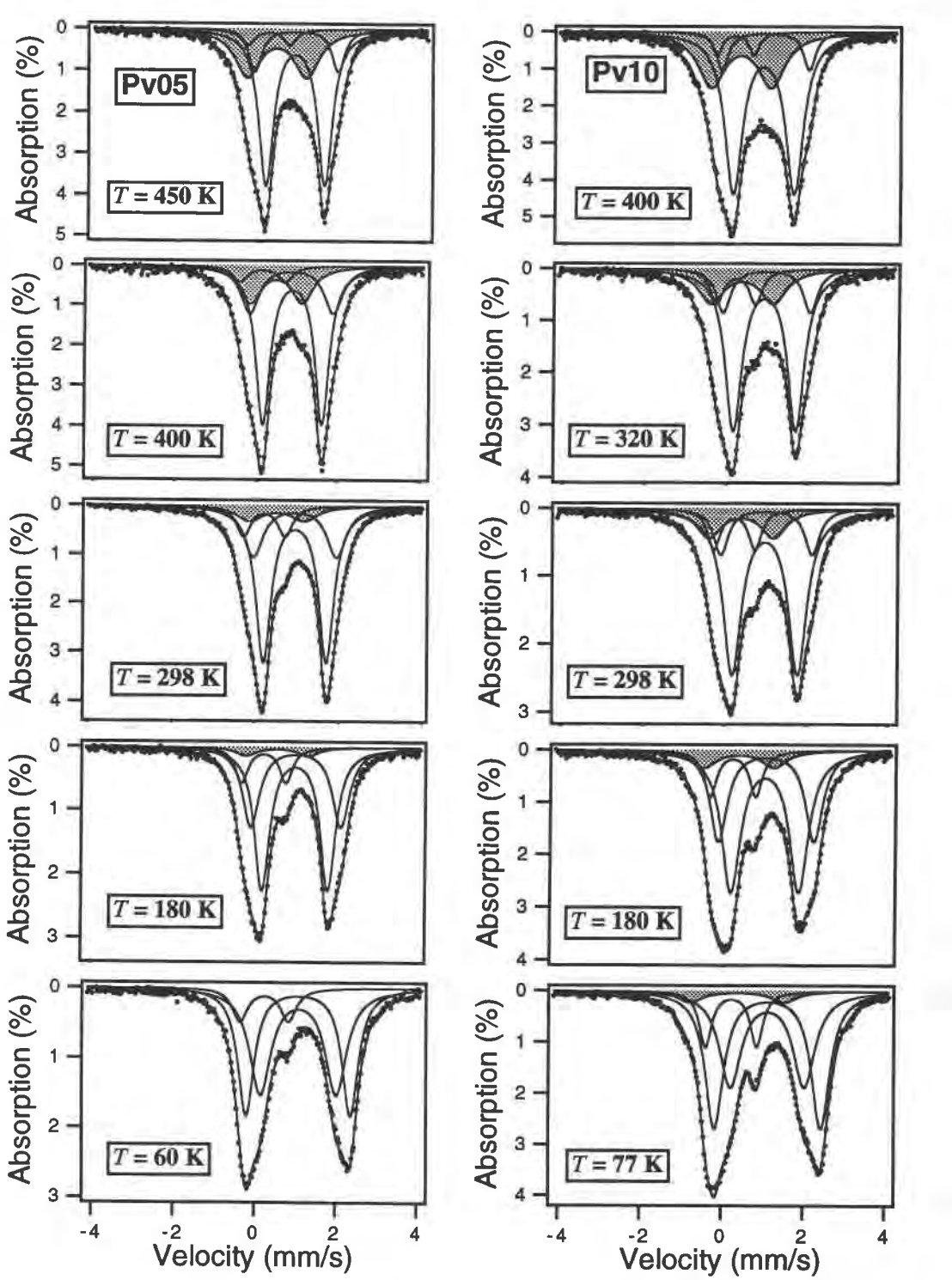

Fig. 5. The ^{57}Fe Mössbauer spectra of $Mg_{0.95}Fe_{0.05}SiO_3$ (labeled as Pv05) and $Mg_{0.9}Fe_{0.1}SiO_3$ (labeled as Pv10) perovskites over the temperature range 60–450 K. The spectra were fitted with two Fe^{2+} doublets, an Fe^{3+} doublet, and a doublet with intermediate hyperfine parameters (Fe^{n+}) (four-doublet model, Tables 4 and 5). See text for discussion. The shaded area indicates the absorption due to electron delocalization. The solid line is the least-squares fitted line assuming Lorentzian line shape to the folded and uncorrected count rates.

TABLE 4. Hyperfine parameters for (Mg,Fe)SiO_3 perovskites as a function of temperature: four-doublet fits

		$Fe^{2+}1$			$Fe^{2+}2$			Fe^{3+}			Fe^{n+}			
No.	T (K)	QS (mm/s)	IS (mm/s)	FWHH (mm/s)	QS (mm/s)	IS (mm/s)	FWHH (mm/s)	QS (mm/s)	IS (mm/s)	FWHH (mm/s)	QS (mm/s)	IS (mm/s)	FWHH (mm/s)	χ^2
							$Mg_{0.90}Fe_{0.10}SiO_3$ (Pv10)							
151P3	450	2.041	1.054	0.350	1.438	1.026	0.491	0.917	0.341	0.266	1.395	0.478	0.833	1.267
149P3	400	2.130	1.098	0.359	1.490	1.058	0.528	0.905	0.355	0.304	1.469	0.488	0.798	1.113
132P3	330	2.130	1.158	0.431	1.528	1.119	0.499	0.951	0.415	0.429	1.575	0.546	0.707	0.973
147P3*	298	2.197	1.178	0.425	1.562	1.138	0.518	0.993	0.416	0.398	1.640	0.535	0.669	1.357
256P1**	298	2.190	1.172	0.430	1.566	1.142	0.542	0.985	0.414	0.402	1.602	0.542	0.593	1.530
131P3	280	2.199	1.179	0.472	1.575	1.151	0.516	1.010	0.404	0.421	1.568	0.556	0.657	1.122
130P3	230	2.236	1.206	0.511	1.586	1.183	0.503	1.057	0.423	0.411	1.639	0.572	0.671	1.283
129P3	181	2.339	1.237	0.507	1.659	1.209	0.562	1.113	0.417	0.370	1.689	0.529	0.701	1.460
128P3	136	2.430	1.267	0.513	1.726	1.240	0.583	1.180	0.422	0.376	2.021	0.526	0.540	1.799
127P3	113	2.482	1.278	0.529	1.762	1.263	0.619	1.233	0.428	0.399	2.281	0.526	0.529	1.750
126P3	86	2.561	1.290	0.513	1.798	1.277	0.658	1.244	0.418	0.368	2.217	0.526	0.563	4.571
260P1**	77	2.550	1.290	0.530	1.774	1.285	0.638	1.237	0.417	0.390	2.290	0.526	0.518	2.580
							$Mg_{0.95}Fe_{0.05}SiO_3$ (Pv05)†							
155P3	450	2.046	1.056	0.382	1.447	1.032	0.443	1.004	0.367	0.302	1.433	0.556	0.762	1.434
153P3	400	2.050	1.037	0.554	1.452	1.068	0.430	1.107	0.311	0.461	1.270	0.648	0.631	1.210
145P3	330	1.951	1.128	0.514	1.480	1.115	0.415	0.980	0.400	0.467	1.392	0.670	0.612	1.030
255P1**	298	2.023	1.140	0.542	1.521	1.132	0.455	0.927	0.427	0.396	1.540	0.554	0.564	1.431
144P3	280	2.019	1.160	0.516	1.527	1.150	0.427	1.023	0.393	0.491	1.413	0.727	0.533	1.155
143P3	230	2.114	1.191	0.540	1.559	1.176	0.429	1.069	0.411	0.460	1.455	0.726	0.488	1.244
142P3	181	2.220	1.221	0.510	1.624	1.205	0.458	1.099	0.425	0.399	1.500	0.726	0.485	1.421

* Spectral data collected with cooling to the cryostat turned off.
** Spectral data collected in a separate experiment.
† Spectral data for Pv05 below 181 K listed in Table 2.

multiple fixed half-width doublets and found that the area ratios of the Fe^{3+}/Fe_{tot}, Fe^{n+}/Fe_{tot}, and Fe^{2+}/Fe_{tot} obtained from the multiple-doublet fits are essentially unchanged from those calculated from the four-doublet fits.

Magnetic relaxation was observed in the spectra of both $Mg_{0.95}Fe_{0.05}SiO_3$ ($T < 50$ K) and $Mg_{0.9}Fe_{0.1}SiO_3$ ($T < 80$ K) perovskites at low temperature. These data are not discussed further, except to note that the onset temperature of magnetic relaxation increases with increasing Fe content of the perovskite.

TABLE 5. Area ratios for (Mg,Fe)SiO_3 perovskites: four-doublet fits

No.	T (K)	$Fe^{2+}1$ (%)	$FE^{2+}2$ (%)	Fe^{3+} (%)	Fe^{n+} (%)	$Fe^{2+}1/Fe^{2+}2$	Fe^{2+} (%)
				$Mg_{0.90}Fe_{0.10}SiO_3$ (Pv10)			
151P3	450	10.24	50.43	3.08	36.20	0.203	60.67
149P3	400	9.39	57.11	4.78	28.70	0.164	66.50
132P3	330	13.91	57.93	11.86	16.30	0.240	71.84
147P3*	298	15.04	59.56	11.06	14.30	0.253	74.60
256P1**	298	13.77	63.36	12.19	10.70	0.217	77.13
131P3	280	18.77	57.43	11.34	12.50	0.327	76.20
130P3	230	28.43	49.39	12.25	9.90	0.576	77.82
129P3	181	30.03	51.15	10.92	7.90	0.587	81.18
128P3	136	36.10	46.60	12.90	4.30	0.775	82.70
127P3	113	40.10	43.20	13.60	3.10	0.928	83.30
126P3	86	43.10	40.60	12.40	3.90	1.062	83.70
260P1**	77	44.70	38.10	13.50	3.50	1.173	82.80
				$Mg_{0.95}Fe_{0.05}SiO_3$ (Pv05)†			
155P3	450	13.08	54.47	3.57	28.88	0.240	67.55
153P3	400	14.08	61.09	4.16	20.66	0.230	75.17
145P3	330	23.56	55.10	12.93	8.41	0.428	78.66
255P1**	298	20.14	61.99	10.86	7.00	0.325	82.13
144P3	280	26.92	53.04	13.74	6.30	0.508	79.96
143P3	230	32.10	51.30	13.43	3.14	0.626	83.40
142P3	181	32.76	52.78	11.57	2.89	0.621	85.54

* Spectral data collected with cooling to the cryostat turned off.
** Spectral data collected in a separate experiment.
† Spectral data for Pv05 below 181 K listed in Table 3.

DISCUSSION

Valence state and site assignments of the quadrupole split doublets

Discrete Fe^{2+} and Fe^{3+} valencies. It was inferred above that the absorption envelope due to Fe^{2+} over the investigated range of temperature is primarily due to next-neighbor configurations, which result in a distribution of the hyperfine parameters. To a first approximation, the fits of the spectral data, given the assumption of two Fe^{2+} quadrupole split doublets, encompass the range of values of the quadrupole splittings and isomer shifts calculated from the multiple-doublet fits to the Fe^{2+} absorption envelope. For both doublets, there is a slight increase in the quadrupole splitting with decreasing temperature that is consistent with the increase normally attributable to Fe^{2+} (Fig. 6). The increase in the isomer shift for the two Fe^{2+} doublets with decreasing temperature for both perovskites (Fig. 7) is consistent with that expected from the second-order Doppler shift.

The Fe^{2+} hyperfine parameters for the perovskite samples at 77 K are compared in Table 1 with the corresponding Fe^{2+} data for orthopyroxene and garnet structures. Values of isomer shift are in the range of 1.26–1.29 mm/s, and quadrupole splittings are in the range of 1.5–2.6 mm/s (Table 4). As noted by McCammon et al. (1992) and Jeanloz et al. (1992), the Fe^{2+} isomer shift for the perovskite structure falls in the range found for the octahedral sites in the orthopyroxene structure (Table 1). However, the assignment of Fe^{2+} to the octahedral sites in the perovskite is inconsistent with the mean M-O bond

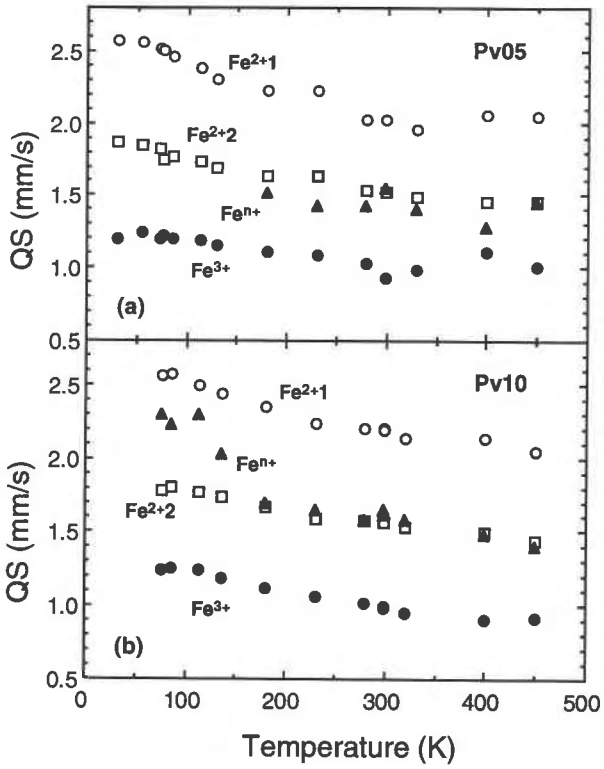

Fig. 6. The quadrupole splittings of the Fe^{3+}, Fe^{n+}, and Fe^{2+} doublets vs. temperature for (a) $Mg_{0.95}Fe_{0.05}SiO_3$ perovskite (labeled as Pv05) and (b) $Mg_{0.90}Fe_{0.10}SiO_3$ perovskite (labeled as Pv10). The open circles, open squares, solid triangles, and solid circles represent the $Fe^{2+}1$, $Fe^{2+}2$, Fe^{n+}, and Fe^{3+} doublets, respectively.

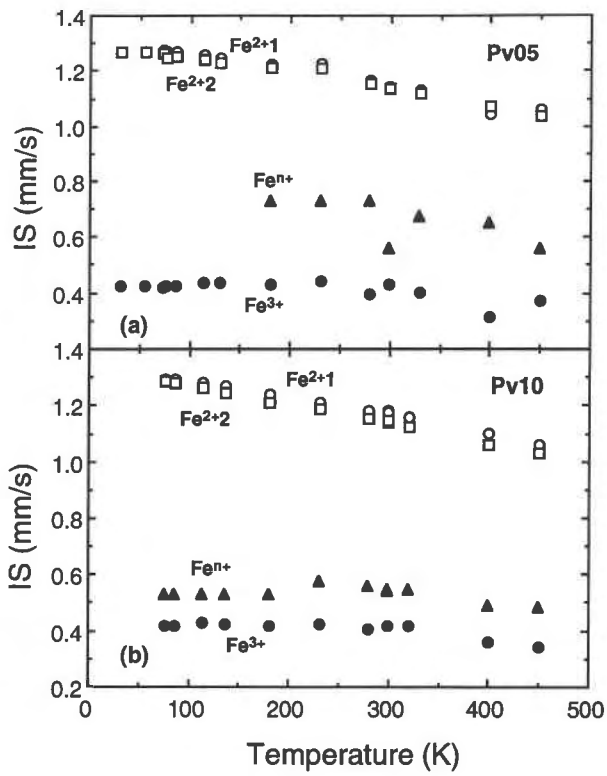

Fig. 7. The isomer shifts of the Fe^{3+}, Fe^{n+}, and Fe^{2+} doublets vs. temperature for (a) $Mg_{0.95}Fe_{0.05}SiO_3$ perovskite (labeled as Pv05) and (b) $Mg_{0.90}Fe_{0.10}SiO_3$ perovskite (labeled as Pv10). The open circles, open squares, solid triangles, and solid circles represent the $Fe^{2+}1$, $Fe^{2+}2$, Fe^{n+}, and Fe^{3+} doublets, respectively.

distances of the octahedral sites, which are significantly smaller in perovskite than in the pyroxene structure. This shorter bond distance should result in smaller values of the isomer shift, possibly <1 mm/s (McCammon et al., 1992). In view of the above argument, it is tentatively concluded that Fe^{2+} occupies the eight- to 12-fold-coordinated site in perovskite. The wide range of values of the Fe^{2+} quadrupole splitting for both perovskites (Table 4) is interpreted to reflect sites of varying degrees of distortion. The assignment of Fe^{2+} to the eight- to 12-fold-coordinated site in perovskite is also consistent with the assignment of bands in the electronic absorption spectra (Shen et al., 1994).

In the fits with four quadrupole split doublets (Table 4), the Fe^{3+} absorption in both perovskite samples is characterized by almost constant values of quadrupole splitting, 0.91–1.23 mm/s (Fig. 6), and values of the isomer shift in the range 0.34–0.43 mm/s as a function of temperature (Fig. 7). The half-width (FWHH) of the absorption doublets is in the range 0.27–0.49 mm/s. These data could be taken as indicating that Fe^{3+} is ordered in a single crystallographic site. The site assignment of Fe^{3+} cannot be determined uniquely from the resonant absorption spectra, but the data are consistent with octahedral coordination. This site assignment is also consistent with the larger M-O distances of the octahedral sites in $Mg_{0.95}Fe_{0.05}SiO_3$ perovskite, as determined from high-resolution X-ray diffraction studies (Finger, 1993 personal communication).

For the $Mg_{0.95}Fe_{0.05}SiO_3$ and $Mg_{0.9}Fe_{0.1}SiO_3$ perovskites, the molar Fe^{3+}/Fe_{tot} calculated from the spectra taken at temperatures <330 K is in the range 0.10–0.13 but systematically decreases at temperatures above 330 K (Fig. 8).

Delocalized Fe^{n+} species. The doublet labeled Fe^{n+} in Tables 4 and 5 and shown shaded in Figure 5 has values of the quadrupole splitting and isomer shift that are intermediate between those assigned to Fe^{2+} and Fe^{3+}. This doublet is first statistically resolved in the spectral data at 77 K in $Mg_{0.9}Fe_{0.1}SiO_3$ perovskite and at 180 K in $Mg_{0.95}Fe_{0.05}SiO_3$ perovskite (Fig. 5). The temperature dependence of the Fe^{n+} hyperfine parameters is shown in Figures 6 and 7. The relative intensity of this doublet increases systematically with increasing temperature (Fig. 8, Table 5). These characteristics are indicative of mixed-valence states that result from a thermally activated electron-delocalization process. As noted above, the increase in the intensity of the Fe^{n+} doublet is matched approximately by a corresponding decrease in the intensity of cumulative Fe^{2+} and Fe^{3+} absorptions (Fig. 8). A decrease in the intensity of the Fe^{3+} absorption in both samples occurs at temperatures above 330 K (Fig. 8).

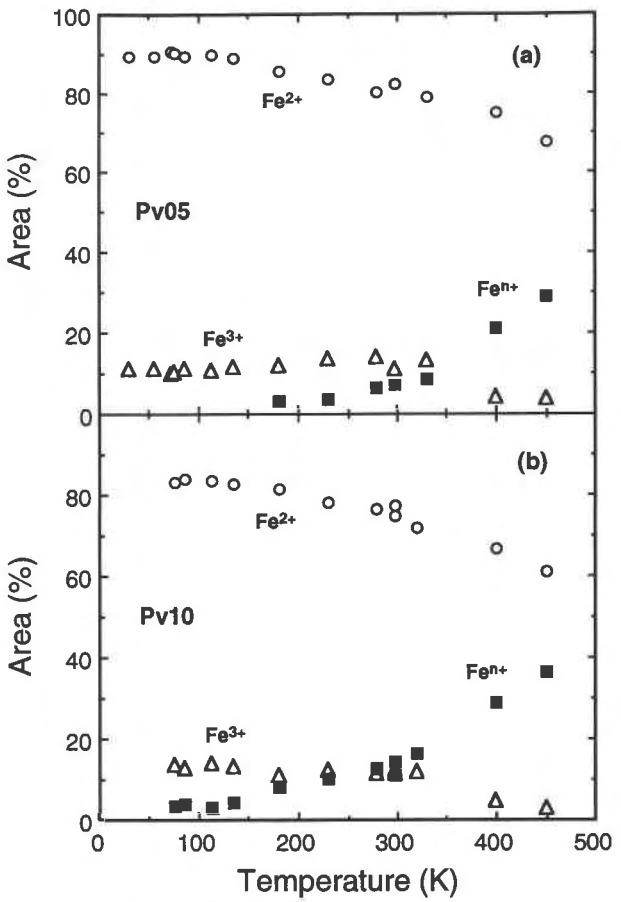

Fig. 8. The Fe^{3+}/Fe_{tot}, Fe^{n+}/Fe_{tot}, and Fe^{2+}/Fe_{tot} area percentages vs. temperature for (**a**) $Mg_{0.95}Fe_{0.05}SiO_3$ perovskite (labeled as Pv05) and (**b**) $Mg_{0.90}Fe_{0.10}SiO_3$ perovskite (labeled as Pv10). The open circles, solid squares, and open triangles represent the Fe^{2+}, Fe^{n+}, and Fe^{3+} species, respectively.

Generally, these intensity changes with temperature are interpreted as a depopulation of electronic levels of the discrete valencies and a population of new delocalized levels associated with intermediate valencies (Burns, 1981, 1991).

The spectral features associated with the electron-hopping process in perovskite can be understood further from a consideration of similar processes in other silicates and oxides. Mixed-valence states that result from thermally activated electron delocalization have been reported in magnetite, ilvaite, cronstedtite, and deerite (Nolet and Burns, 1979; Evans and Amthauer, 1980; Amthauer et al., 1980; Coey et al., 1982; Amthauer and Rossman, 1984; Burns, 1981, 1991, 1993). In each of these minerals, the electron delocalization is restricted to infinite edge-sharing octahedra, which form chains in magnetite or ribbons in ilvaite and deerite. In high-temperature Mössbauer spectra, the electron delocalization is observed as a sharp absorption pattern with intermediate hyperfine parameters, either as a magnetic Zeeman pattern in magnetite or as a quadrupole split doublet in ilvaite and deerite (Evans and Amthauer, 1980; Amthauer et al., 1980). In each of these examples, all the Fe on the crystallographically equivalent sites is involved in electron exchange between Fe^{2+} and Fe^{3+}. At lower temperatures (below 400 K), the electron delocalization in ilvaite and deerite is associated with a broader absorption doublet, with intermediate hyperfine parameters, in addition to absorption doublets due to frozen-in Fe^{2+} and Fe^{3+} valencies (Nolet and Burns, 1979; Evans and Amthauer, 1980; Amthauer and Rossman, 1984). In Zn-, Ti-, and Fe-bearing spinels, electron delocalization is unequivocally observed as a continuous absorption envelope between the high-velocity Fe^{2+} and Fe^{3+} absorption lines in the temperature-dependent Mössbauer spectra (Lotgering and van Diepen, 1977). In this case, the continuous absorption is explained by a thermally activated electron exchange and by a nonequivalence of the octahedral sites occupied by Fe^{2+} and Fe^{3+}. The nonequivalence of the sites is attributed to different next-nearest neighbor populations, which result in potential energy differences between the sites. The observation of superimposed, localized Fe^{2+} and Fe^{3+} species, in addition to the continuous absorption in the spectra of spinels, implies that the electron exchange occurs for only part of the Fe^{2+}-Fe^{3+} pairs. Similar findings are also reported in aegerine-augite, wherein at low concentrations of Fe^{2+} there are only a few isolated Fe^{2+}-Fe^{3+} pairs in a matrix of Fe^{3+} ions in the M1 chain (Amthauer and Rossman, 1984).

In many ways, the temperature-dependent changes in the resonant absorption of perovskite that are associated with electron delocalization are similar to that found in the spinel structure discussed above. The half-width of the absorption doublet associated with electron delocalization increases with increasing temperature (Table 4). The fitting of a single broad absorption doublet of Lorentzian line shape (Fig. 5) may be only an approximation to the real model of the spectral data. Because the absorption due to Fe^{2+} in perovskite reflects next-nearest neighbor sites, the alternative explanation is that the Fe^{2+}-Fe^{3+} pairs have a broad variety of electron-delocalization energies leading to continuous absorption in the spectra.

Several other features of the absorption associated with electron delocalization in perovskite are explained qualitatively by the Lotgering and van Diepen (1977) model for spinels. In their model, the exchange frequency between localized Fe^{2+} and Fe^{3+} ions passes the critical value of 10^8/s, the inverse mean lifetime of the excited Fe nucleus, at a particular temperature. With increasing temperature, the critical value of the exchange frequency is then matched by pairs of sites with increasing potential energy differences. An increasing number of Fe^{2+}-Fe^{3+} pairs contribute to the absorption associated with electron delocalization. In principle, the relative intensity of the Fe^{n+} doublet, corresponding to the proportion of Fe sites that participate in the electron-delocalization process, increases with increasing temperature (cf. Fig. 8). Also, with similar molar Fe^{3+}/Fe_{tot}, the fraction of the number of Fe ions involved in the exchange process in-

creases with increasing Fe content at any given temperature. Figure 8 shows that the relative intensity of the Fe^{n+} doublet is greater in $Mg_{0.9}Fe_{0.1}SiO_3$ perovskite than in $Mg_{0.95}Fe_{0.05}SiO_3$ perovskite at any given temperature. Increasing the hopping frequency is expected to result in a sharp resonance associated with electron exchange. In perovskite, the absorption associated with the electron exchange remains broad even at 450 K, which suggests that the frequency of the electron-hopping process does not greatly exceed the critical value of 10^8/s.

Almost all the minerals that exhibit Fe^{2+}-Fe^{3+} exchange attributable to electron delocalization have structures wherein Fe^{2+} and Fe^{3+} randomly occupy infinite edge-shared polyhedra (Burns, 1981, 1991, 1993; Amthauer and Rossman, 1984). The Fe^{2+}-Fe^{3+} distances are in the range 2.7–3.2 Å. In aegerine-augite, where the Fe^{2+}/Fe^{3+} is low, the percentage of Fe sites that participate in the exchange process is much lower than, for example, in magnetite, ilvaite, and deerite. Amthauer and Rossman (1984) explained the low percentage of Fe sites involved in electron exchange in terms of a perturbation of the electron-delocalization process by next-nearest cation neighbors. In other silicates such as vivianite, lazulite, rockbridgeite, and babingtonite, there is no evidence for mixed-valence states of Fe, even though the Fe^{2+}-Fe^{3+} distances are in the range 2.7–3.3 Å. This absence of mixed-valence states is attributed to structures where the Fe-bearing polyhedra form only small clusters of two, three, or four octahedra (Amthauer and Rossman, 1984). Burns (1981) cites a few examples of minerals wherein the electron exchange involves crystallographically distinct cation sites. One example is Fe^{2+}-Fe^{3+} exchange between the edge-sharing cube and tetrahedra (M-M distance of ~3.1 Å) in the Fe- and Ti-containing garnets. Another example is electron delocalization by means of edge-sharing octahedra-tetrahedra in cordierite (M-M distance of 2.74 Å).

In the $MgSiO_3$-perovskite structure, it is well established that Si and Mg cations occupy the sixfold-coordinated octahedra and the eight- to 12-fold-coordinated polyhedra, respectively (e.g., Horiuchi et al., 1987; Kirkpatrick et al., 1991). The structure is composed of a three-dimensional network of corner-sharing octahedra. By rotation and displacement of the octahedra, the interstices among the octahedra form distorted polyhedra with the coordination number 8–12 (e.g., Horiuichi et al., 1987). In the structure, the sixfold-coordinated octahedra share all corners. The octahedra and eight- to 12-fold-coordinated polyhedra share all their edges with each other, with an M-M distance ranging from 2.79 to 3.24 Å (Ross and Hazen, 1990). The adjacent polyhedra are face-sharing, with M-M distances from 3.35 to 3.52 Å (Ross and Hazen, 1990). Electron-transfer processes in perovskite, therefore, are limited to cations in either crystallographically face-sharing, nonequivalent octahedra-polyhedra or face-sharing polyhedra. Transitions between face-sharing octahedra-polyhedra perhaps are favored over those between the face-sharing polyhedra because the former are associated with the shortest metal-metal distance. On the other hand, extensive electron delocalization in oxides and silicates has only been observed between cations in crystallographically equivalent sites. In the perovskite structure, the prevailing evidence is for Fe^{2+} to occupy the eight- to 12-fold-coordinated sites. On the basis of the powder diffraction measurements on the $Mg_{0.95}Fe_{0.05}SiO_3$ perovskite (Finger, 1993 personal communication), Fe^{3+} probably is ordered on the octahedrally coordinated sites. An electron-hopping mechanism that involves the face-sharing octahedra-polyhedra is therefore proposed. These polyhedra also have the shortest M-M distances.

Implications for the electrical conductivity of the lower mantle

Measurements of the electrical conductivity of lower-mantle phases are relevant to understanding further the internal electromagnetic processes such as the transmission of geomagnetic signals from the Earth's interior (Burns, 1993). In this connection, recent measurements of the electrical conductivity of Fe-bearing perovskite have generated some degree of controversy (e.g., Li et al., 1993; Poirier and Peyronneau, 1992). Specifically, the ambient-temperature electrical conductivity of perovskite and a mixture of $(Mg,Fe)SiO_3$ perovskite and magnesiowüstite, (Mg,Fe)O, measured by Li and Jeanloz (1990) is lower by about three orders of magnitude than those reported by Poirier and Peyronneau (1992). The results of Poirier and Peyronneau, extrapolated to lower-mantle pressures, are in agreement with the value of 1 S/m at a depth of 1000 km, determined from the analysis of the transient and secular variations of the geomagnetic field. In light of the results of this study, it is of interest that Poirier and Peyronneau (1992) appealed to a conduction mechanism in perovskite that involves electron hopping between Fe^{2+} and Fe^{3+} to explain their high conductivity. The present ^{57}Fe Mössbauer results support this proposal. Poirier and Peyronneau (1992) reported activation energies of conduction in the range 0.21–0.35 eV, decreasing with increasing Fe content. In comparison, Litterst and Amthauer (1984) and Ghazi-Bayat et al. (1992) reported values of the activation energy of 0.11–0.25 eV for the hyperfine fluctuations due to electron hopping in natural and Mn-substituted synthetic monoclinic ilvaite. Activation energies for conduction in ilvaite in the range 0.13–0.24 eV were reported by Grandjean and Gerard (1975), Heilmann et al. (1977), and Coey et al. (1984). Activation energies of 0.12 eV were also reported by Lotgering and van Diepen (1977) for the electron exchange in Zn-bearing spinel. In these studies of electron hopping, the similarities of the activation energies of conduction and electron exchange are notable.

Although the activation energies of the electron exchange process in some silicates and oxides are of the appropriate order of magnitude to explain the conduction mechanism in perovskite, there remain a number of uncertainties with this comparison. As discussed by Wood

and Neil (1991), the oxidation state is of prime importance in controlling both the conduction mechanism and the electrical conductivity. The perovskite samples synthesized under different conditions have different Fe^{3+} content. The Fe^{3+}/Fe_{tot} of the two perovskite samples discussed in this study are the highest (about 0.12) of any perovskites so far discussed in the literature. The perovskite sample used in the study of McCammon et al. (1992) was synthesized in the presence of Fe metal. The Fe^{3+}/Fe_{tot} value of 0.05 determined from their Mössbauer spectra at 77 K, therefore, represents the minimum Fe^{3+} content in perovskite, with Fe/(Mg + Fe) of 0.053. A significantly lower Fe^{3+}/Fe_{tot} value (<0.01) was reported by Jeanloz et al. (1992) for a $Mg_{0.9}Fe_{0.1}SiO_3$ perovskite synthesized in diamond-anvil cell by laser heating. Therefore, the discrepancy in the measured electrical conductivities of perovskite may be partly explained by an electron-hopping conduction mechanism. Another factor that deserves attention is that the activation energy associated with the electron exchange process in spinel and ilvaite may be different from that in perovskite because in the former cases the Fe^{2+}-Fe^{3+} pairs occur in crystallographically equivalent octahedra that share edges to form infinite chains or ribbons. In the perovskite structure, the Fe^{2+}-Fe^{3+} pairs most likely form clusters within the three-dimensional polyhedral framework. The cooperative electron exchange is likely to be higher in the latter case, even in samples with low Fe^{3+}/Fe_{tot}. It is evident from the above discussion that additional studies of the electron exchange and the conduction processes in well-characterized perovskite samples are warranted.

Acknowledgments

We are thankful for the constructive reviews of C.A. McCammon and the late R.G. Burns. This work was supported by the NSF grant (EAR-9005228), the NSF Science and Technology Center for High Pressure Research (EAR-8920239), and the Carnegie Institution of Washington.

References cited

Amthauer, G., and Rossman, G.R. (1984) Mixed valence of iron in minerals with cation clusters. Physics and Chemistry of Minerals, 11, 37–51.

Amthauer, G., Langer, K., and Schliestedt, M. (1980) Thermally activated electron delocalization in deerite. Physics and Chemistry of Minerals, 6, 19–30.

Burnham, C.W., Ohashi, Y., Hafner, S.S., and Virgo, D. (1971) Cation distribution and atomic thermal vibrations in an iron-rich orthopyroxene. American Mineralogist, 56, 850–876.

Burns, R.G. (1981) Intervalence transitions in mixed-valence minerals of iron and titanium. Annual Review of Earth and Planetary Sciences, 9, 345–383.

——— (1991) Mixed valency minerals: Influences of crystal structures on optical and Mössbauer spectra. In K. Prassides, Ed., Mixed valence systems: Applications in chemistry, physics and biology, p. 175–200. Plenum, New York.

——— (1993) Mineralogical application of crystal field theory, 551 p. Cambridge University Press, Cambridge, U.K.

Coey, J.M.D., Moukarika, A., and McDonagh, C.M. (1982) Electron hopping in cronstedtite. Solid State Communications, 41, 797–800.

Coey, J.M.D., Allan, J., Xuemin, K., Van Dang, N., and Ghose, S. (1984) Magnetic and electrical properties of ilvaite. Journal of Applied Physics, 55, 1963–1965.

Evans, B.J., and Amthauer, G. (1980) The electronic structure of ilvaite and the pressure and temperature dependence of its ^{57}Fe Mössbauer spectrum. Journal of Physics and Chemistry of Solids, 41, 985–1001.

Fei, Y., Wang, Y., Virgo, D., Mysen, B.O., and Mao, H.K. (1992) Ferric iron in (Mg,Fe)SiO_3-perovskite: A Mössbauer spectroscopic study (abs.). Eos, 73 (14), 300.

Ghazi-Bayat, B., Behruzi, M., Litterst, F.J., Lottermoser, W., and Amthauer, G. (1992) Crystallographic phase reansition and valence fluctuation in synthetic Mn-bearing ilvaite $CaFe^{2+}_{2-x}Mn^{2+}_xFe^{3+}[Si_2O_7/O/(6OH)]$. Physics and Chemistry of Minerals, 18, 491–496.

Grandjean, F., and Gerard, A. (1975) Analysis by Mössbauer spectroscopy of the electronic hopping process in ilvaïte. Solid State Communications, 16, 553–556.

Heilmann, I.U., Olsen, N.B., and Olsen, J.S. (1977) Electron hopping and temperature dependent oxidation states of iron in ilvaite studied by Mössbauer effect. Physics Scripta, 15, 285–288.

Horiuchi, H., Ito, E., and Weidner, D.J. (1987) Perovskite-type $MgSiO_3$: Single crystal X-ray diffraction study. American Mineralogist, 72, 357–360.

Ito, E., and Matsui, Y. (1978) Synthesis and crystal-chemical characterization of $MgSiO_3$ perovskite. Earth and Planetary Science Letters, 38, 443–450.

Jackson, W.E., Knittle, E., Brown, G.E., Jr., and Jeanloz, R. (1987) Partitioning of Fe within high-pressure silicate perovskite: Evidence for unusual geochemistry in the lower mantle. Geophysical Research Letters, 14, 224–226.

Jeanloz, R., and Thompson, A.B. (1983) Phase transitions and mantle discontinuities. Review in Geophysics and Space Physics, 21, 51–74.

Jeanloz, R., O'Neill, B., Pasternak, M.P., Taylor, R.D., and Bohlen, S.R. (1992) Mössbauer spectroscopy of $Mg_{0.9}Fe_{0.1}SiO_3$ perovskite. Geophysical Research Letters, 19, 2135–2138.

Kirkpatrick, R.J., Howell, D., Phillips, B.L., Cong, X.D., Ito, E., and Navrotsky, A. (1991) MAS NMR spectroscopic study of $Mg^{29}SiO_3$ with the perovskite structure. American Mineralogist, 76, 673–676.

Kudoh, Y., Prewitt, C.T., Finger, L.W., Darovskikh, A., and Ito, E. (1990) Effect of iron on the crystal structure of (Mg,Fe)SiO_3 perovskite. Geophysical Research Letters, 17, 1481–1484.

Li, X., and Jeanloz, R. (1990) Laboratory studies of the electrical conductivity of silicate perovskites at high pressures and high temperatures. Journal of Geophysical Research, 95, 5067–5078.

Li, X., Ming, L., Manghnani, M.H., Wang, Y., and Jeanloz, R. (1993) Pressure dependence of the electrical conductivity of $(Mg_{0.9}Fe_{0.1})SiO_3$ perovskite. Journal of Geophysical Research, 98, 501–508.

Litterst, F.J., and Amthauer, G. (1984) Electron delocalization in ilvaite, a reinterpretation of its ^{57}Fe Mössbauer spectrum. Physics and Chemistry of Minerals, 10, 250–255.

Liu, L.G., and Bassett, W.A. (1986) Elements oxides, silicates, 250 p. Oxford University Press, New York.

Lotgering, F.K., and van Diepen, A.M. (1977) Electron exchange between Fe^{2+} and Fe^{3+} ions on octahedral sites in spinels by means of paramagnetic Mössbauer spectra and susceptibility measurements. Journal of Physics and Chemistry of Solids, 38, 565–572.

Luth, R.W., Virgo, D., Boyd, F.R., and Wood, B.J. (1990) Ferric iron in mantle-derived garnets. Contributions to Mineralogy and Petrology, 104, 56–72.

McCammon, C.A., Rubie, D.C., Ross, C.R., II, Seifert, F., and O'Neill, H.St.C. (1992) Mössbauer spectra of $^{57}Fe_{0.05}Mg_{0.95}SiO_3$ perovskite at 80 and 298 K. American Mineralogist, 77, 894–897.

Nolet, D.A., and Burns, R.G. (1979) Ilvaite: A study of temperature dependent electron delocalization by the Mössbauer effect. Physics and Chemistry of Minerals, 4, 221–234.

Parise, J.B., Wang, Y., Yeganeh-Haeri, A., Cox, D.E., and Fei, Y. (1990) Crystal structure and thermal expansion of (Mg,Fe)SiO_3 perovskite. Geophysical Research Letters, 17, 2089–2092.

Poirier, J.B., and Peyronneau, J. (1992) Experimental determination of the electrical conductivity of the material of the Earth's lower mantle. In Y. Syono and M.H. Manghnani, Eds., High-pressure research in mineral physics: Applications to Earth and planetary sciences, p. 77–78. Terra Scientific, Tokyo.

Ross, N.L., and Hazen, R.M. (1990) High-pressure crystal chemistry of $MgSiO_3$ perovskite. Physics and Chemistry of Minerals, 17, 228–237.

Shen, G., Fei, Y., Hålenius, U., and Wang, Y. (1994) Optical absorption spectra of (Mg,Fe)SiO_3 silicate perovskites. Physics and Chemistry of Minerals, 20, 478–482.

Smyth, J.R., and Bish, D.L. (1988) Crystal structures and cation sites of the rock-forming minerals, p. 332. Allen and Unwin, Boston, Massachusetts.

Stevens, I.G., and Stevens, V.E. (1972) Mössbauer effect data index, covering the 1970 literature IFI/Plenum Data Corporation.

Virgo, D., and Hafner, S.S. (1969) Fe^{2+}-Mg order-disorder in heated orthopyroxenes. Mineralogical Society of America Special Paper, 2, 67–81.

Wang, Y., Guyot, F., and Liebermann, R.C. (1992) Electron microscopy of (Mg,Fe)SiO_3 perovskite: Evidence for structural phase transitions and implications for the lower mantle. Journal of Geophysical Research, 97, 12327–12347.

Wood, B.J., and Neil, J. (1991) High-temperature electrical conductivity of the lower-mantle phase (Mg,Fe)O. Nature, 351, 309–311.

Yagi, T., Mao, H.K., and Bell, P.M. (1978) Structure and crystal chemistry of perovskite-type $MgSiO_3$. Physics and Chemistry of Minerals, 3, 97–110.

Manuscript received September 21, 1993
Manuscript accepted May 4, 1994